Pergamon

Cement and Concrete Research 33 (2003) 679–687

CEMENT AND CONCRETE RESEARCH

Induced anisotropic permeability due to drying of concrete

Nicolas Burlion[a,b,*], Frédéric Skoczylas[a,c], Thierry Dubois[a,c]

[a]*Laboratory of Mechanics of Lille, UMR 8107, France*
[b]*Polytech'Lille–USTL, Dpt GTGC, Cité Scientifique, Villeneuve d'Ascq Cedex 59650, France*
[c]*Ecole Centrale de Lille BP 48, Cité Scientifique, Villeneuve d'Ascq Cedex 59651, France*

Received 19 March 2002; accepted 22 October 2002

Abstract

Structural strength, porous space, and permeability of concrete are strongly affected by mechanical, hydrous, and thermal loading. These various loadings may lead to drying shrinkage, one of the main characteristics of this type of material, which has to be involved in the behaviour modelling and experimental investigations being the subjects of this paper. Experimental devices and principal parameters studied are first presented. Drying shrinkage and loss of mass in time were measured on prismatic samples while uniaxial compression tests were performed on cylindrical samples. Gas permeability tests, carried out on a concrete cylinder 30 mm in diameter, form the second part of this study. The samples used for these measurements were cored from each prismatic sample at the end of 10 months or 2 years of drying, either from the transverse direction of sample (privileged direction of drying) or from the longitudinal direction. Gas permeability procedure, using micropulse test technique, is described as well as the experimental process. Experimental results are finally commented on and discussed with a view on induced anisotropy due to desiccation. Such an anisotropy is clearly observable in permeability, which is also increasing with drying time.

Keywords: Durability; Drying; Microcracking; Gas permeability; Anisotropy

1. Introduction

This study outlines the effects of drying shrinkage and the induced damage of concrete material upon its gas permeability. As a consequence of its low cost and its ability to be formed, concrete is widely used even if the ageing process of the material is complex. This process leads to a change in mechanical and hydraulic behaviour, in chemical properties, and in saturation level. These changes are obviously linked to material and structure surround. Under drying conditions, free interstitial water can evaporate. Thus, the cementitious matrix is subjected to tensile stresses, which may induce microcracks when the material tensile strength is exceeded [1–3]. The knowledge of its ageing process and its consequences upon the properties, mentioned above, is crucial for material intended for use in the manufacture of containers for highly radioactive elements. For confining or water-retaining structures, permeability is one of the most important properties that has been the subject of numerous studies [4–6]. From an experimental perspective, degradations in concrete modulus or strength, and the corresponding change in water and gas permeability due to static loading and microcracking, have been demonstrated and documented in the literature [6–8]. It was also shown that parameters, such as the crack network connectivity and its opening, have an influence on concrete permeability.

Furthermore, one of the main requirements for concrete containment structure is low concrete permeability (to prevent environmental pollution), as this quality is indicative of the concrete durability [9]. In the mean time and even if only superficially observable [10,11], microcracks of the cement paste are induced by drying and desiccation shrinkage (Fig. 1). Bisschop and van Mier showed recently that microcracks due to drying were diffused in the material, if the size of aggregates is larger than 6 mm, due to a size effect upon an aggregate-restraining mechanism. However, this induced microcracking is almost homogeneous, whatever the structural effect on drying process is [12–14]. This induced microcracking will lead to an increase in permeab-

* Corresponding author. Polytech'Lille-USTL, Dpt GTGC, Cité Scientifique, Villeneuve d'Ascq Cedex 59650, France. Tel.: +33-320-43-45-61; fax: +33-328-76-73-01.
E-mail address: Nicolas.Burlion@eudil.fr (N. Burlion).

0008-8846/02/$ – see front matter © 2002 Elsevier Science Ltd. All rights reserved.
doi:10.1016/S0008-8846(02)01039-6

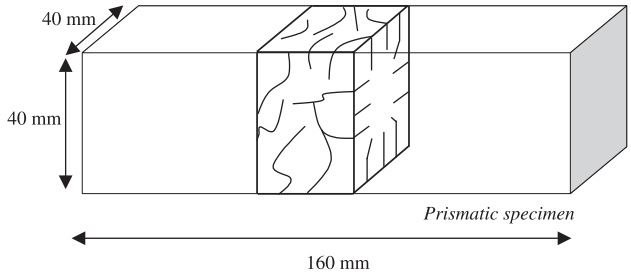

Fig. 1. Possible crack pattern due to drying and desiccation shrinkage [14].

ility, which is generally assumed to be isotropic [15–17], especially when drying occurs from heat treatment [18]. On the other hand, concrete structures exhibit a main drying direction, which is often along their smallest size, i.e., along the highest hydrous gradient. To verify whether the permeability variations are isotropic or not, gas permeability measurements were carried out on a concrete submitted to natural drying for 10 months or 2 years. In these tests, two different permeabilities were measured: along the highest hydrous gradient direction, or the perpendicular one.

This study is divided in two parts. The first part is devoted to the drying process that induces microcracks. The used concrete and its curing conditions are described. Loss in mass and shrinkage measurements were carried out to evaluate the direct drying effects, and also the mechanical uniaxial tests, at the end of different times in order to point out the effect of induced drying microcracking on mechanical properties. Over a 10-month period—larger than the time required to achieve the measurable drying shrinkage—two smaller samples were cored from each specimen used for the previously mentioned measurements. These were intended for gas permeability tests that make up the second part of the study. An anisotropic variation of permeability, induced by drying and desiccation shrinkage, can be observed. The drying time effects are then described and commented on.

2. Microfissuration development: experimental investigation on drying shrinkage

2.1. Material and specimen design

The whole shrinkage of concrete is composed of several parts [3,19,20]; the influence of each depends on the concrete composition [1,21–23]: endogenous shrinkage, thermal shrinkage, and desiccation shrinkage. Thermal shrinkage is due to the cooling process after cement hydration. Self-desiccation shrinkage comes from internal drying by consuming water in pores during hydration. Endogenous shrinkage is the sum of Le Châtelier contraction and self-desiccation shrinkage [24–27]. Finally, desiccation shrinkage is induced by the imbalance between the heart and the surface sample, leading to the leak-off of free water from concrete. A compressive deformation of skeleton material due to an increase of capillary pressure is then observed [3]. Other authors assign desiccation shrinkage to surface tension [20] or disjoining pressures phenomena [28]. However, the shrinkage deformation is partially prevented by both gravels and heterogeneous hygrometric states in concrete body. Since tensile stress takes place in cement matrix, there is initiation and propagation of microcracks when the material strength is exceeded. Influences of such microcracks on mechanical behaviour and gas permeability in both drying directions are visible and presented in this paper.

In order to capture this desiccation process and its consequences, a specific laboratory testing procedure was designed and the concrete material was compounded in order to maximise shrinkage deformation in a relatively short time. As there is a relationship between drying shrinkage and water/cement ratio [23,29], a high ratio value was chosen. Thus, such a material would exhibit a high initial permeability facilitating leak-off of water from sample. Moreover, a strong shrinkage should be observed in concrete with a small diameter of the biggest gravel and a high water/cement ratio. As a consequence, a 8-mm diameter of the biggest gravel and a W/C ration of 0.6 were used. The cement is CEM II/B-M (LL-S) 32.5 R CP2 (in European norm EN 197-1). The composition of the concrete is then 324 kg/m^3 cement, 205 kg/m^3 water, 1110 kg/m^3 4/8 mm gravel, and 668 kg/m^3 0/4 mm sand, giving an actual W/C ratio of 0.63. This composition is used in order to obtain a uniaxial compression strength less than 30 MPa at 28 days. With such a W/C ratio, the cement matrix structure is formed of large-diameter pores [22,23,30] and allows a high-drying kinetics. After 28 days, the porous cement structure is completed [19], which lets us assume that hydric exchange will occur with a quasi-constant porosity for each specimen.

Measurements of shrinkage have to be made on small-sized samples, like on our $40 \times 40 \times 160$ mm^3 prismatic specimens. The self-desiccation shrinkage occurring mainly during hydration [3,24] can be neglected after 28 days. This has been confirmed in Ref. [23] where endogenous shrinkage ended after 28 days while drying shrinkage continued to progress. Colina and Acker [10] showed that temperature of a 1-m-sized cube was steady after 31 days. Assuming that the temperature will remain constant, after 28 days in our specimens, is then consistent and allows the thermal shrinkage to be ignored.

The specimens were preserved during 28 days in a pool at a 20 °C constant temperature. In order to avoid the portlandite dissolution by water, the prismatic specimens were let inside plastic bags emerged in water. After 28 days of curing, the specimens are taken off the water and submitted to a relative humidity of $60 \pm 5\%$ and a temperature of 21 ± 1 °C.

Even if there is an asymptotic stabilisation of desiccation shrinkage after 90 days [23,31], drying will continue [3]. The scale effect should also be taken into account in the shrinkage phenomenon [1,31,32] since the internal varia-

tions of hydrous states are dependent on sample size. The larger the structure size is, the slower the hydrous state changes are. On the other hand, there is a rapid variation of water content in structures with small characteristic size. Accordingly, the effect of drying shrinkage on the mechanical behaviour of concrete may be observable on small-sized structures only [3,31].

2.2. Desiccation shrinkage results: its influence on microcracks

To take into account the curing procedure, the complete saturation of samples was initially assumed. The water content is then deduced from the loss in mass of specimens. Fig. 2 shows the evolution of shrinkage strain versus time of drying. Fig. 3 depicts the evolution of shrinkage strain for three specimens in relation to the loss in mass during 70 days of drying. The results are similar to those obtained by Granger et al. [32]. Two phases can be put forward. The first part of the curves corresponds to the rapid drying of the specimen surface, which leads to superficial microcracking delaying the global shrinkage evolution. In the second phase, the proportionality between loss in mass and shrinkage strain brings to light the effect of drying on concrete. If the measurement was continued after 70 days, a third phase would be obtained where the shrinkage strain would tend to stabilise while the loss in mass continues to evolve.

Uniaxial compression tests were performed on the same concrete at the end of different times of drying. During drying, water content is no longer uniform in the specimen: this leads to the definition of an overall elastic stiffness of specimen rather than the elastic modulus of concrete material. This elastic stiffness is strongly influenced by growth of microcracks during drying shrinkage. In order to compare results obtained from different specimens, a dimensionless initial stiffness was used. It is given by the stiffness measured from the third loading–unloading cycle in each test (the corresponding axial stress is 9 MPa), which is normalised by the maximal value of this initial stiffness obtained from all specimens. Fig. 4 shows the evolution of

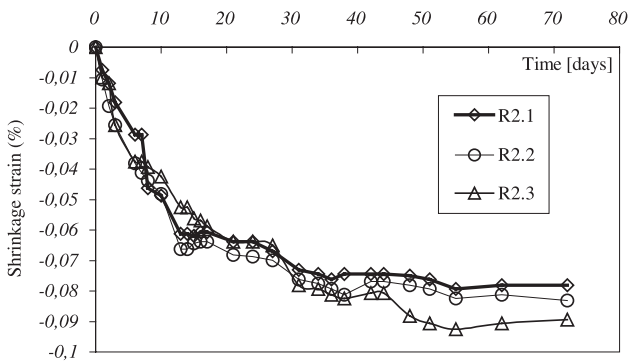

Fig. 2. Evolution of shrinkage strain versus time for three prismatic specimens.

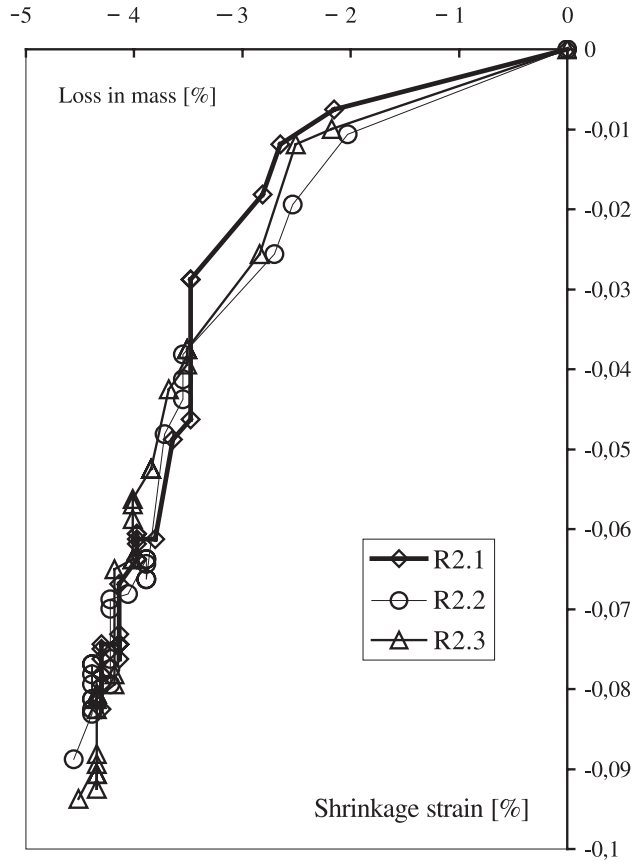

Fig. 3. Evolution of shrinkage versus the loss in mass for three prismatic specimens.

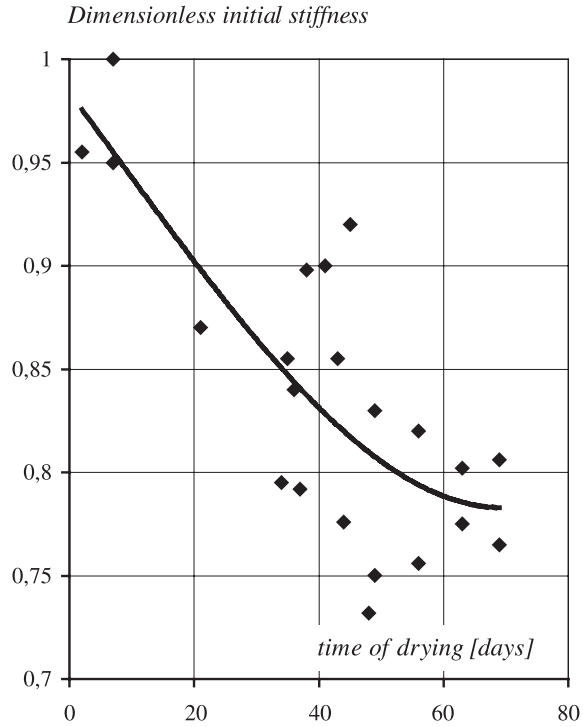

Fig. 4. Evolution of dimensionless initial stiffness versus time of drying.

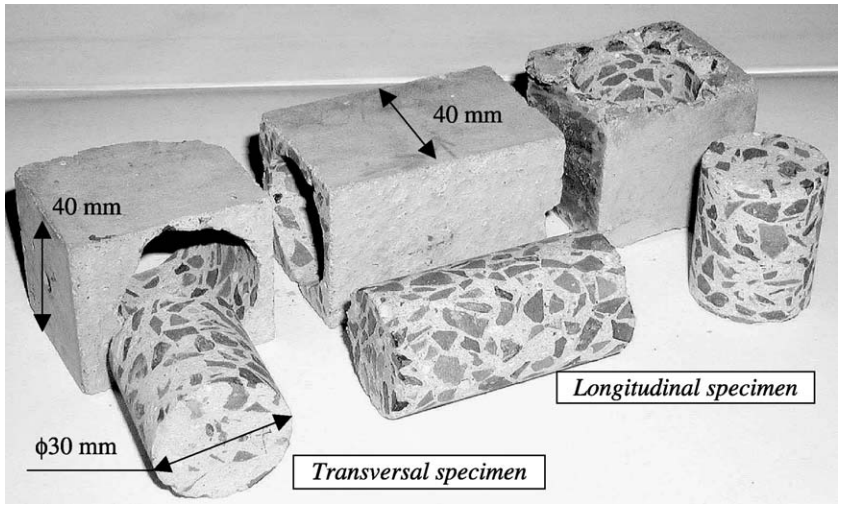

Fig. 5. Photograph of specimens.

dimensionless initial stiffness of cylinders (220 mm height, diameter 110 mm) relative to the time of drying. Each mark is the average value of two tests performed on the same day. It is clear that the drying process, showing a decrease in elastic stiffness of concrete, induces microcracks. Furthermore, induced drying microcracks lead to changes in the behaviour of concrete, which becomes more brittle than in saturated cases [33].

2.3. Specimens for permeability measurements

While modifying the concrete mechanical behaviour, microcracking will certainly have an influence on its permeability. In order to show a possible anisotropy of permeability induced by a desiccation process, cylindrical samples 30 mm in diameter were cored from those used for the previous tests. Before coring, six prismatic samples were kept under the conditions mentioned before (Section 2.1) for 10 months (three prismatic samples denoted S1–S3) and 2 years (denoted S4–S6). Those corings were carried out along the longitudinal and transversal sizes, respectively, of the prismatic sample (Fig. 5). The 30-mm samples were then stuck into a 66-mm-diameter metallic tube, with Araldite glue (Fig. 6). This specific preparation allows the sample to be used in the triaxial cell of our laboratory.

Fig. 6. Photograph of permeability specimens.

3. Gas permeability measurements: influence of microcracking induced by drying

3.1. General principles of gas permeability measurements

In the following, we present the experimental method aimed at measuring the gas permeability of the material. The injected gas is argon U of above 99% purity, which will be considered as a perfectly pure gas in the rest of the study. The general principle of testing conditions is to subject the cylindrical sample to a low confining pressure and static gas pressure on its upper and lower surfaces, to apply a slight excess of pressure to one of the sides, and to record over a period of time the evolution in the difference of pressure between the two surfaces. This test is similar to a low-amplitude pulse test [34]. The experimental apparatus used is shown in Fig. 7.

This assembly comprises:

- A confining cell
- A Gilson pump and a digital manometer capable of applying the confining pressure
- A gas injection circuit comprising:
  - An argon supply reservoir and a high-pressure reducer manometer
  - Two surge reservoirs R_1 and R_2 (the sample is placed between the two)
  - A digital manometer for measuring the static pressure
  - A transmitter and a differential pressure indicator to apply and measure the difference in pressure between both sides of the sample

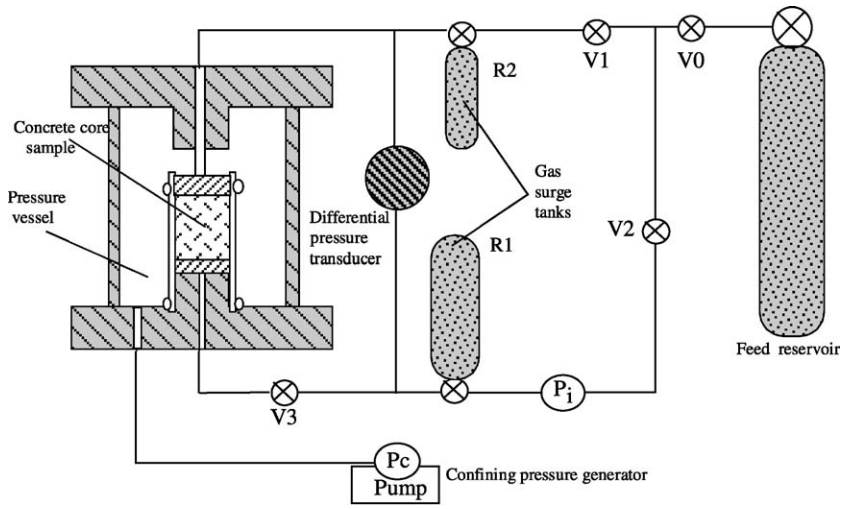

Fig. 7. Diagram showing experiment and equipment.

- A plotting table or a computer for recording the difference in pressure between both sides of the sample over a period of time.

3.2. Testing boundary conditions

The sample and the tube are placed inside the cell and subjected to the confining pressure, fixed at 3 MPa. The static pressure $P_i = 2$ MPa is then applied to both faces; the two reservoirs are at the same pressure and are connected by opening valves V_1, V_2, and V_3. After a 3-h wait, required for balancing the internal pressures, the two injection circuits are isolated by closing valves V_1 and V_3. A slight excess in injection pressure ΔP_1 is applied to reservoir R_1 and valve V_3 is opened to allow the gas to be diffused over the whole sample. Evolution $[P_2(t) - P_1(t)] = \Delta P(t)$ can then be measured and read on the differential pressure indicator. We have chosen an excess pressure $\Delta P_1 = 0.05$ MPa. This value lies within the range of generally accepted excess pressures [35,36]. Fig. 8 gives a highly simplified representation of the experiment and enables us to indicate the boundary conditions for this test.

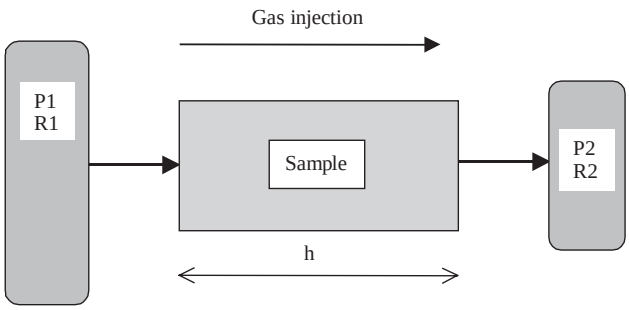

Fig. 8. Experimentation conditions.

The boundary conditions are:

- At time $t < 0$, $P_2 = P_1 = P_i$.
- At time $t = 0$, $P_1 = P_i + \Delta P_1$, $P_2 = P_i$.
- At time $t > 0$, $P_1 = P_1(t)$, $P_2 = P_2(t)$.
- At final time, $P_2 = P_1 = P_f$.

3.3. Hypotheses and data processing

In this study, it is supposed that the fluid flow obeys Darcy's law. The flow is sufficiently slow to be considered as laminar and the static pressure is sufficiently high for the Klinkenberg effect [37] to be ignored. In such a case, it can be written as:

$$\vec{V} = -\frac{K}{\mu}\overrightarrow{\mathrm{grad}}\,P \tag{1}$$

K is thus the permeability of the medium to gas [m^2] and μ is the viscosity of argon. Taking into account the mass balance equation and ignoring the effects of poromechanical coupling on the fluid pressure because of the high level of the latter's compressibility, the well-known diffusivity equation is obtained:

$$\frac{K}{\mu}\mathrm{div}(P\overrightarrow{\mathrm{grad}}\,P) = \phi\frac{\partial P}{\partial t} \tag{2}$$

ϕ is the porosity of the material, which remains free for the circulation of gas.

During the test, the only measurements available are the variations of pressure in the reservoirs $P_1(t)$, $P_2(t)$, and $\Delta P(t)$. To find permeability K using such measurements, two methods can be envisaged: a numerical analysis using, e.g., the finite element method [34], or a simplified method, originally described by Brace and Walsh [38]. In this case, we have chosen the second method. The basic

hypothesis is that this transient state (pulse test) is formed of a succession of steady states with the following boundary conditions:

- $P_1 = P_1(t)$ at $x = 0$.
- $P_2 = P_2(t)$ at $x = h$.

Since the pulse amplitude is very low compared to the initial static pressure, it can be shown [39], at this stage, that:

$$P_1(t) - P_2(t) = \Delta P(t) = \Delta P_1 \exp(-cP_f t) \text{ with}$$
$$c = -\frac{KA}{\mu h}\left(\frac{1}{V_1} + \frac{1}{V_2}\right) \quad (3)$$

where P_f is the final static pressure at the end of the pulse test, and V_1 and V_2 are the volumes of the buffer reservoirs.

This result is used to calculate permeability K by comparing this theoretical drop in pressure and the real measurement, as well as by choosing coefficient c, which gives the theoretical value closest to the measured value.

3.4. Results in anisotropic permeability measurements

Fifteen permeability measurements were performed on six different samples submitted to either a 10-month period or 2 years of drying. Notice that the prismatic samples were made up the same day. As mentioned before, two or three smallest cylinders were cored from each prismatic sample—one along the longitudinal direction, and one or two along the transversal direction (highest hydrous gradient direction). This allowed two different permeabilities K_L (longitudinal permeability) and K_T (transversal permeability), respectively, to be measured in order to assess a possible microcracking anisotropy and its consequence upon material permeability. The results of measurements, carried out after 10 months of drying, are given in Table 1.

As the permeability range is measured from 2.9×10^{-16} to 6.8×10^{-16} m^2, these results show that this property is almost homogeneous for the tested concrete. Except for sample S2, a significant difference between longitudinal and transversal permeabilities cannot be observed even if the latter are slightly higher than the longitudinal values. This phenomenon can be due, at least in part, to surface microcracking with low connectivity. Microcracks are certainly formed, but either in insufficient number or with an opening that is too weak for the permeability to increase significantly. This second point has to be underlined and related to experiments previously performed in our laboratory [40]. The aim of these tests was to clarify experimentally the respective roles of mechanical damage (i.e., microcracking) and the degree of microcracks opening on the increase in permeability. The variation of that was continuously recorded under triaxial compression loading (open cracks) and after unloading (closed cracks). Considerable differences were observed and showed that permeability is highly conditioned by the degree to which the microcracks have opened at a given damage level. As a conclusion, these slight differences in transversal and longitudinal permeabilities have to be confirmed by other tests carried out on older specimens; these differences could be amplified if the material is subjected to a deviatoric loading (likely to lead to an opening of microcracks).

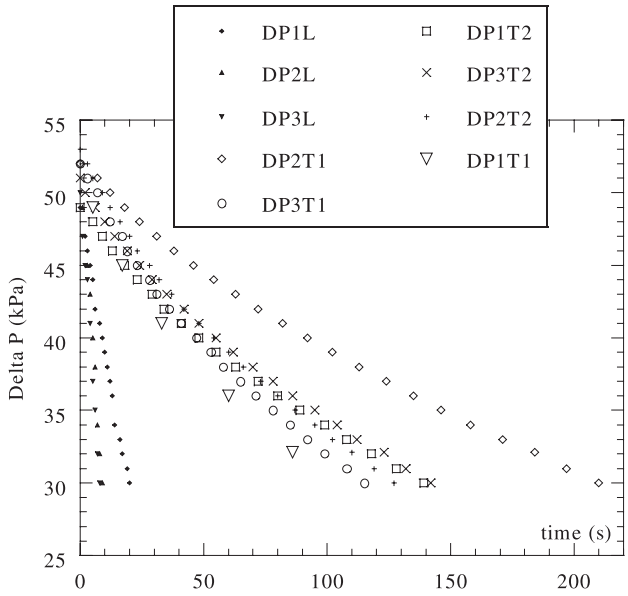

Fig. 9. Drop in pressure difference recording.

Thus, nine complementary tests were performed after a 2-year period of drying. Two transversal cylinders and one longitudinal cylinder (same sizes as before) were cored from the three prismatic samples (S4–S6; Fig. 5) and tested under the same previously mentioned conditions. As an example, evolutions of pressure differences are plotted Fig. 9. Results are given in Table 2 and, as is made clear by this table, they are not those expected. It is striking that the first tendency now inverted as longitudinal permeability is higher than the

Table 1
Results on permeability measurements after 10 months of drying

Sample number	K_L (m^2)	K_T (m^2)	K_T/K_L
S1	5.0×10^{-16}	5.0×10^{-16}	1.00
S2	3.9×10^{-16}	6.8×10^{-16}	1.74
S3	2.9×10^{-16}	3.4×10^{-16}	1.17
Average	3.9×10^{-16}	5.0×10^{-16}	1.31

Table 2
Permeability results at the end of 2 years of drying

Sample number	K_L (m^2)	K_T (m^2)		K_T/K_L
		K_{T1} (m^2)	K_{T2} (m^2)	
S4	1.0×10^{-14}	0.20×10^{-14}	0.14×10^{-14}	0.17
S5	2.6×10^{-14}	0.10×10^{-14}	0.16×10^{-14}	0.05
S6	2.5×10^{-14}	0.19×10^{-14}	0.14×10^{-14}	0.066
Average	2.03×10^{-14}	0.16×10^{-14}	0.15×10^{-14}	0.076

transversal one (one order of magnitude). When compared to the six previous experiments, the results show undeniable drying and/or drying time effects.

- A significant increase of permeability during the complementary drying process: This increase may be attributed to two phenomena—a decrease of the moisture content however the loss in mass from 10 months to 2 years of drying was very low and a probable continuation of the microcracking process leading to a more connected and opened cracked network.
- An actual permeability anisotropy with a K_L/K_T ratio varying from 5 to 20: As already underlined, this ratio was unexpected because we thought the drying effect would have been more pronounced along the transversal direction.

As it is reported in the literature, there is often a large scattering of the permeability values of samples coming from different specimens of the same concrete (differences in cure conditions, saturation degree, etc.). In fact, if the values presented in Table 1 are not significantly different, the tendency seems to be an increase in transversal permeability compared to the longitudinal one. Nevertheless, it is very clear that this tendency is totally inverted for samples after 2 years of drying. As the three permeabilities (S4*L*, S4*T1*, and S4*T2*) are measured on specimens cored from the same prismatic sample (see Fig. 5), any statistical effect should not be suspected. Furthermore, even if coming from three different prismatic samples, the longitudinal permeabilities are systematically higher than the transversal one, with a K_L/K_T ratio being of one order of magnitude; at the same time, the three longitudinal values can be considered as almost identical (varying from 1.0×10^{-14} to 2.6×10^{-14} m^2) while there is no significant scattering of transversal values (varying from 0.10×10^{-14} to 0.20×10^{-14} m^2).

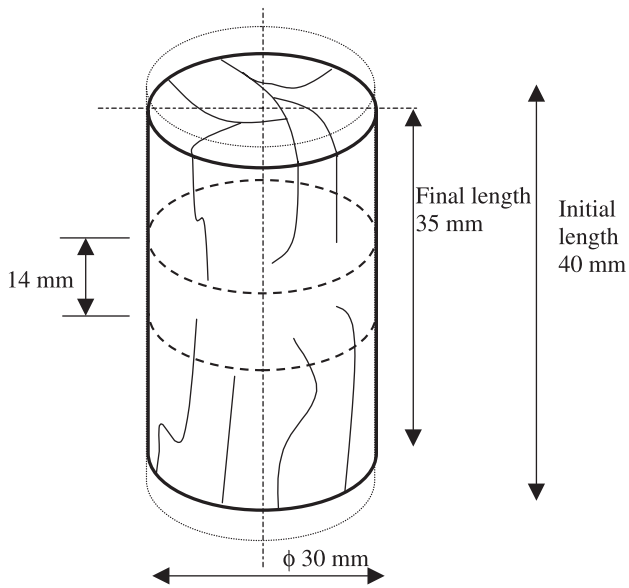

Fig. 10. Transversal cylindrical specimen for measurement of gas permeability.

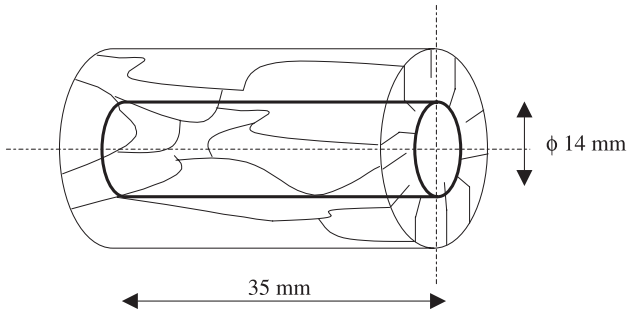

Fig. 11. Recored longitudinal cylindrical specimen for measurement of gas permeability in the central part.

In the absence of complete clarification, new experimental investigations, using previously tested samples S6*L* (longitudinal specimen issued from sample S6) and S6*T2* (one of the transversal specimen from S6), were decided. The main purpose of this complementary study was to investigate whether the cracked network is deep or not and the "degree" of connectivity of such cracks. A central slice (14 mm thickness) (Fig. 10) was thus cut out from sample S6*T2* and a smaller cylinder (14 mm diameter) recored from sample S6*L* (Fig. 11). The permeability values are summarised in Table 3.

The first observation is that permeabilities of entire or recored S6*L* cylinders are virtually the same. That means that a deep and connected cracked network took place inside the specimen—a network which we suspect to be radial, as represented in Fig. 11. A way to verify (almost in part) this assumption was to submit this recored sample (whose preparation is the same as illustrated Fig. 6) to a high confining pressure of 55 MPa, leading (after a rapid calculation) to about a 12-MPa radial stress on the concrete sample. The effect is significant as there is an important permeability decrease now being 0.40×10^{-14} m^2 (see Table 3). This is an evidence that a connected microcracked network is present, as our own laboratory experiences (in such measurements on confined rocks) have always shown a low confining pressure effect (upon permeability) on safe rocks (without significant presence of cracks).

The second observation is that the central part of sample S6*T2* exhibits a higher permeability than the end parts but lower than the longitudinal value (recored or not). Thus, anisotropy is confirmed, even for the sample heart, and there is a visible "skin" effect that induces a drop of permeability. This effect could be due to carbonation [41,42], as it is

Table 3
Permeability results on complementary tests

Sample S6	K_L (m^2)	K_{T2} (m^2)
S6*L* (entire)	2.50×10^{-14}	
S6*L* (recored)	1.60×10^{-14}	
S6*L* (recored and stressed)	0.40×10^{-14}	
S6*T2* (entire)		0.14×10^{-14}
S6*T2* (central part)		0.44×10^{-14}

frequently reported in the literature as lowering concrete or mortar permeability. Carbonation was not actually measured. According to the literature on a similar concrete [43], deepness of carbonation can be estimated to a maximum of 10 mm in such sample conservation mode after 2 years. Furthermore, specimens were cut according to Fig. 10 in order to avoid some edge effects. Thus, the remaining carbonated thickness can be assumed to be approximately 7 mm.

4. Conclusions

In this study, we have shown the influence of desiccation-induced microcracking on mechanical properties and the gas permeability of concrete. Test results of drying shrinkage were presented and correlated with the stiffness loss of cylindrical concrete specimens submitted to uniaxial compression (about 20%). An induced microcracking of the material leads to an increase of gas permeability. In a second part, we have pointed out the existence of an induced anisotropy in terms of permeability. Several important points were put in evidence, as follows.

- The induced anisotropy in gas permeability of concrete was not that expected. It traduces the fact that microcracks occur, in a first time, preferentially along the highest drying gradient induced by the structure geometry. Nevertheless, this anisotropy is relatively slight when material is unloaded. In a second time, the opening, the length, and the connectivity of cracks become important and lead to an increase in the longitudinal permeability. As for the transverse permeability, microcracks do not completely cross the sample—what gives lower permeability.
- The radial microcracking (parallel to the higher hydrous gradients), whose length and connectivity increase during drying, has an important effect in terms of global permeability increase.
- The effect of the suspected carbonation remains beneficial for the permeability of concrete, in spite of the drying microcracking effect. Moreover, the heart of the sample is more permeable than its skin.
- The effect of confining pressure leads to a partial closure of microcracks created by the drying process. An additional prestressing of concrete structure could decrease gas permeability (see, e.g., nuclear protection problems).
- From a modelling point of view, taking into account this decrease of permeability for numerical calculations in long-term durability analysis would be useful, while keeping in mind that longitudinal permeability, along a wall for example, may become higher than the transversal one.

References

[1] Z.P. Bazant, F.H. Wittmann (Eds.), Creep and Shrinkage in Concrete Structures, Wiley, London, 1982.
[2] Z.P. Bazant, W.J. Raftshol, Effect of cracking in drying and shrinkage specimens, Cem. Concr. Res. 12 (1982) 209–226.
[3] P. Acker, Comportement mécanique du béton: apports de l'approche physico-chimique (in French), Thèse de doctorat de l'Ecole Nationale des Ponts et Chaussées, Paris, Rapport de Recherche LPC 152, 1988.
[4] B. Gérard, H.W. Reinhardt, D. Breysse, Measured transport in cracked concrete, in: H.W. Reinhardt (Ed.), Penetration and Permeability of Concrete: Barriers to Organic and Contaminating Liquids, E&FN Spon, UK, 1997, pp. 265–324.
[5] K. Wang, D. Jansen, S.P. Shah, A. Karr, Permeability study of cracked concrete, Cem. Concr. Res. 27 (3) (1997) 381–393.
[6] C.-M. Aldea, S.P. Shah, A. Karr, Permeability of cracked concrete, Mater. Struct. 32 (1999) 370–376.
[7] H.R. Samaha, K.C. Hover, Influence of microcracking on the mass transport properties of concrete, ACI Mater. J. 89 (4) (1992) 416–424.
[8] B. Gérard, J. Marchand, Influence of cracking on the diffusion properties of cement-based materials: Part I. Influence of continuous cracks on the steady-state regime, Cem. Concr. Res. 30 (1) (2000) 37–43.
[9] J.-M. Torrenti, O. Didry, J.-P. Ollivier, F. Plas (Eds.), La Dégradation des Bétons, Couplage Fissuration–Dégradation Chimique, Hermès, Paris, 1999, in French.
[10] H. Colina, P. Acker, Drying cracks: kinematics and scale laws, Mater. Struct. 33 (2000) 101–107.
[11] H. Sadouki, F.H. Wittmann, Shrinkage and internal damage induced by drying and endogeneous drying, in: V. Baroghel-Bouny, P.-C. Aïtcin (Eds.), Shrinkage of Concrete, RILEM Publications PRO 17, Paris, France, 2000, pp. 299–314.
[12] J. Bisschop, J.G.M. van Mier, Meso-level mechanisms of drying shrinkage cracking in concrete, Proceedings of the International RILEM Workshop on Fracture and Durability, Post-Conference Workshop of Framcos IV, Cachan, France, June 1, 2001.
[13] J. Bisschop, L. Pel, J.G.M. van Mier, Effect of aggregate size and paste volume on drying shrinkage microcracking in cement-based composites, in: F. Ulm, Z.P. Bazant, F.H. Wittmann (Eds.), Creep, Shrinkage and Durability Mechanics of Concrete and Other Quasi-Brittle Materials, Elsevier, Amsterdam, 2001, pp. 75–80.
[14] J. Bisschop, J.G.M. van Mier, How to study drying shrinkage microcracking in cement-based materials using optical and scanning electron microscopy? Cem. Concr. Res. 32 (2) (2002) 279–287.
[15] F. Jacobs, Permeability to gas of partially saturated concrete, Mag. Concr. Res. 50 (2) (1998) 115–121.
[16] A. Abbas, M. Carcasses, J.-P. Ollivier, Gas permeability of concrete in relation to its degree of saturation, Mater. Struct. 32 (1999) 3–8.
[17] V. Picandet, A. Khelidj, G. Bastian, Effect of axial compressive damage on gas permeability of ordinary and high-performance concrete, Cem. Concr. Res. 31 (11) (2001) 1525–1532.
[18] N. Hearn, Effect of shrinkage and load-induced cracking on water permeability of concrete, ACI Mater. J. 96 (2) (1999) 234–241.
[19] P.-C. Aïtcin, A. Neville, P. Acker, Les différents types de retrait du béton (in French), Bull. Lab. Ponts Chaussées 215 (4184) (1998) 41–51.
[20] F.H. Wittmann, Creep and shrinkage mechanisms, in: Z.P. Bazant, F.H. Wittmann (Eds.), Creep and Shrinkage in Concrete Structures, Wiley, London, 1982, pp. 129–161.
[21] F. de Larrard, R. Le Roy, Relation entre formulation et quelques propriétés mécaniques des bétons à hautes performances (in French), Mater. Struct. 25 (1992) 464–475.
[22] V. Baroghel-Bouny, Caractérisation microstructurale et hydrique des pâtes de ciment et des bétons ordinaires et à très hautes performances (in French), Thèse de doctorat de l'Ecole Nationale des Ponts et Chaussées, Paris, 1994.
[23] V. Baroghel-Bouny, P. Rougeau, S. Care, J. Gawsewitch, Etude comparative de la durabilité des bétons B30 et B80: I. Microstructure, propriétés de durabilité et retrait (in French), Bull. Liaison Lab. Ponts Chaussées 217 (4204) (1998) 61–73.
[24] C. Hua, Analyses et modélisations du retrait d'autodessiccation de la pâte de ciment durcissante (in French), Thèse de doctorat de l'Ecole Nationale des Ponts et Chaussées, Paris, 1992.
[25] L. Granger, J.-M. Torrenti, M. Diruy, Simulation numérique du retrait

du béton sous hygrométrie variable, Bull. Liaison Lab. Ponts Chaussées 190 (3811) (1994) 57–64 (in French).
[26] Z.P. Bazant, Criteria for rational prediction of creep and shrinkage of concrete, Rev. Fr. Genie Civ. 3 (3–4) (1999) 61–89.
[27] F.-J. Ulm, F. Le Maou, C. Boulay, Creep and shrinkage coupling: new review of some evidence, Rev. Fr. Genie Civ. 3 (3–4) (1999) 21–37.
[28] Z.P. Bazant, Nonlinear water diffusion in nonsaturated concrete, Mater. Struct. 5 (1972) 3–20.
[29] S.E. Pihlajavaara, Estimation of drying of concrete at different relative humidities and temperatures of ambient air with special discussion about fundamental features of drying and shrinkage, in: Z.P. Bazant, F.H. Wittmann (Eds.), Creep and Shrinkage in Concrete Structures, Wiley, London, 1982, pp. 87–108.
[30] H.W. Reinhardt, Relation between the microstructure and structural performance of concrete, in: A. Aguado, R. Gettu, S.P. Shah (Eds.), Technology Transfer on the New Trend in Concrete, Proceedings of ConTech '94, Barcelona, 1994, pp. 19–32.
[31] S.E. Pihlajavaara, A review of some of the main results of a research on the ageing phenomena of concrete, effect of moisture conditions on strength, shrinkage and creep of mature concrete, Cem. Concr. Res. 4 (5) (1974) 761–771.
[32] L. Granger, J.-M. Torrenti, P. Acker, Thoughts about drying shrinkage: scale effects and modelling, Mater. Struct. 30 (1997) 96–105.
[33] F. Bourgeois, N. Burlion, J.F. Shao, Modelling of elastoplastic damage in concrete due to desiccation shrinkage, Int. J. Numer. Anal. Methods Geomech. 26 (2002) 759–774.
[34] F. Skoczylas, J.-P. Henry, A study of intrinsic permeability to gas, Int. J. Rock Mech. Min. Sci. Geomech. Abstr. 32 (2) (1995) 171–179.
[35] J.D. Walls, Effects of pore pressure, confining pressure and partial saturation on permeability of sandstones, PhD Thesis, Stanford University, 1982.
[36] J. Walder, A. Nur, Permeability measurement by the pulse-decay method: effect of poroelastic phenomena and non-linear pore pressure diffusion, Int. J. Rock Mech. Min. Sci. Geomech. Abstr. 23 (3) (1986) 225–232.
[37] R. Iffly, Etude de l'écoulement des gaz dans les milieux poreux (in French), Rev. IFP 11 (6) (1956) 757–796.
[38] W.F. Brace, W.T. Walsh, Permeability of granite under high pressure, J. Geophys. Res. 73 (6) (1968) 2225–2236.
[39] E. Dana, F. Skoczylas, Gas relative permeability and pore structure of sandstones, Int. J. Rock Mech. Min. Sci. 36 (5) (1999) 613–625.
[40] H. Meziani, F. Skoczylas, An experimental study of the mechanical behaviour of a mortar and its permeability under deviatoric loading, Mater. Struct. 32 (1999) 403–409.
[41] A.M. Neville, Properties of Concrete, 4th ed., Longman, New York, USA, 1995.
[42] A. Castel, G. Arliguie, T. Chaussadent, V. Baroghel-Bouny, La microfissuration superficielle a-t-elle une influence sur la profondeur de carbonatation des bétons? (in French), Rev. Fr. Genie Civ. 5 (2–3) (2001) 231–248.
[43] R. Duval, La durabilité des armatures et du béton d'enrobage, in: J. Baron, J.-P. Ollivier (Eds.), La Durabilité des Bétons, Presses de l'Ecole Nationale des Ponts et Chaussées, Paris, 1996, pp. 173–225 (in French).